Supporting Information for "How does seismic rupture accelerate? Observational insights from earthquake source time functions"

Julien Renou[1], Martin Vallée[1], Pierre Dublanchet[2]

[1]Institut de Physique du Globe de Paris, Université de Paris, CNRS Paris, France

[2]MINES ParisTech, PSL Research University, Centre de Géosciences, Fontainebleau, France

Contents of this file

1. Text S1 to S2
2. Figures S1 to S13

Introduction These supplementary materials first include Text S1 and the associated Figure S1(a), detailing the method used to estimate the confidence intervals of the parameters relating moment acceleration to moment rate. Confidence intervals for the parameters of the time evolution of the moment rate are then computed and shown in Figure S1(b). Text S2 and the associated Figure S2 explain how the synthetic catalog of bimodal STFs is generated, with the aim of reproducing the main shape of the SCARDEC STFs. The independency between the moment acceleration and final magnitude is shown for all the prescribed moment rates in Figures S3 to S12. Finally, the relation between moment acceleration and moment rate, for lower and upper limits of the development phase at $0.05F_m$ and $0.5F_m$, respectively, is shown in Figure S13.

Text S1: Statistical analysis for m, β, n_d and α_d values

In this section we show how the confidence intervals for the fitting parameters m, β, n_d and α_d are obtained. For that, we consider the 40 prescribed moment rates (see main text for details). For each moment rate, we randomly select 75 different $(\ddot{M}_d)_{ij}$ values, so that we consider the same number of observations for small and large moment rates (as $N_{40} = 75$). Then a linear fit (in log-log scale) is performed for the 75×40 data points extracted, providing a first possible m and a first $b = \log \beta$. We iterate the procedure of moment acceleration selection and (m, b) estimation 10000 times so that we end up with 10000 (m, b) couples characterizing the 10000 subsets of 75×40 data points extracted from the initial data. We then compute the joint probability density function for m and b, and derive the corresponding confidence map shown in Figure S1(a). The confidence map for n_d and α_d shown in figure S1(b) is obtained following the same procedure, after converting the m and b samples to n_d and $\log \alpha_d$ samples. Note that $\log \beta$ and $\log \alpha_d$ show a negative correlation with m and n_d, respectively. The confidence intervals provided in the main text have been estimated from the marginal densities, and should therefore be interpreted according to this trade-off.

Text S2: Setting-up of the synthetic STFs catalog

We build our catalog of synthetic STFs by combining the macroscopic properties found by past studies with the observed time evolution of the development phase. Intrinsic complexity of the rupture propagation, which leads to the exact shape of each individual STF, prevents from the constitution of a fully realistic synthetic STF catalog. However, diversity in terms of STFs shape can be mainly characterized, for a given seismic moment M_0, by a source duration with a log-normal distribution and a variable number of local

peaks. We first generate for each bin of M_w a log-normal distribution of source durations T_i, with a mean $T_0 = 4.5 \cdot 10^{-6}(M_0)^{1/3}$ (self-similar equation of GCMT (Ekström et al., 2012)) and a standard deviation $\sigma = 0.37$ ((Courboulex et al., 2016)). We then build for each T_i bimodal STFs, with two sub-events growing as $\dot{M}_d(t) = \alpha_k t^{n_k}$. The first sub-event always starts at time 0 and its growing phase randomly stops between 0 and the half total duration $T_i/2$. Duration of the growing phase of the second sub-event is also randomly selected between 0 and $T_i/2$ but its start is adapted such as the growing phase ends at $T_i/2$. α_i and n_i values for each STF randomly vary around their observational values (8.8×10^{16} and 2.68 respectively). The first subevent has a linear decline with the same duration as its growth while the second subevent always declines linearly from $T_i/2$ to T_i. Figure S2 shows an example of how an STF is built with the constraints detailed above.

References

Courboulex, F., Vallée, M., Causse, M., & Chounet, A. (2016). Stress-drop variability of shallow earthquakes extracted from a global database of source time functions. *Seismological Research Letters*, *87*(4), 912–918.

Ekström, G., Nettles, M., & Dziewoński, A. (2012). The global cmt project 2004–2010: Centroid-moment tensors for 13,017 earthquakes. *Physics of the Earth and Planetary Interiors*, *200*, 1–9.

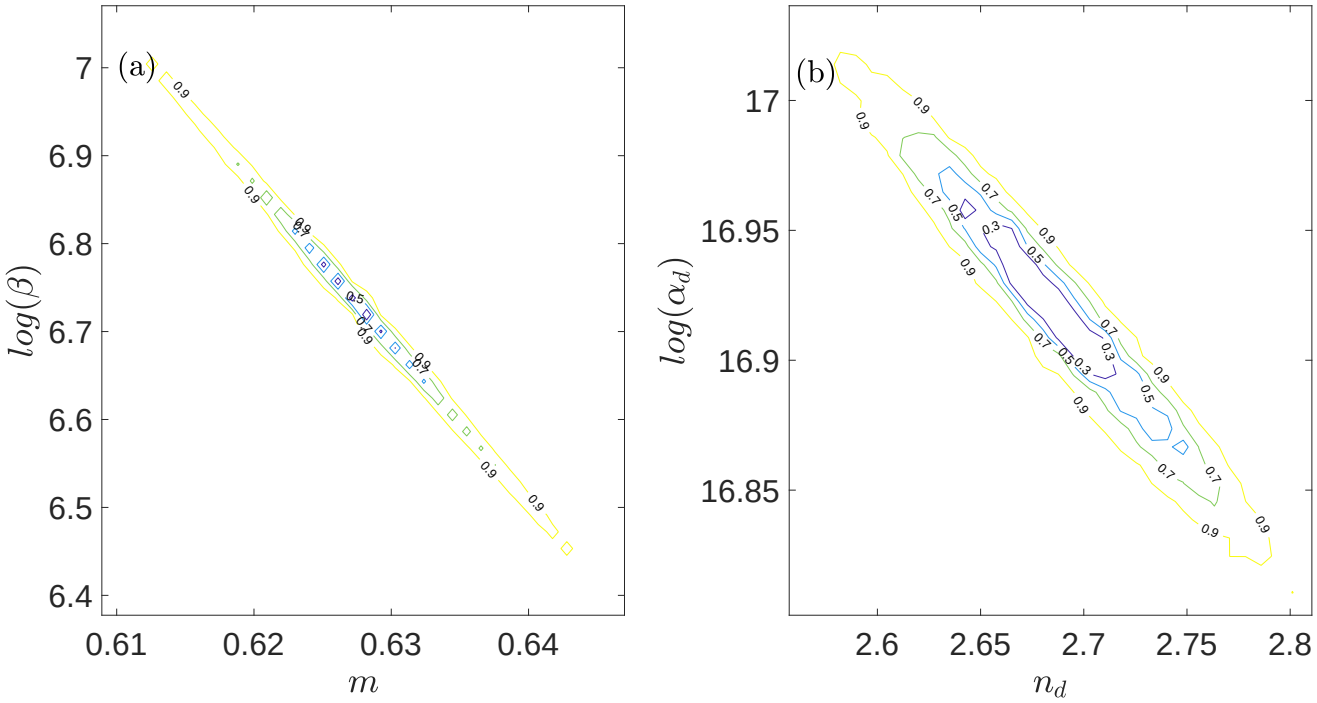

Figure S1. Confidence maps for $(m, b = \log \beta)$ parameters (a), and $(n_d, \log \alpha_d)$ (b). The labels on the contours indicate the confidence level.

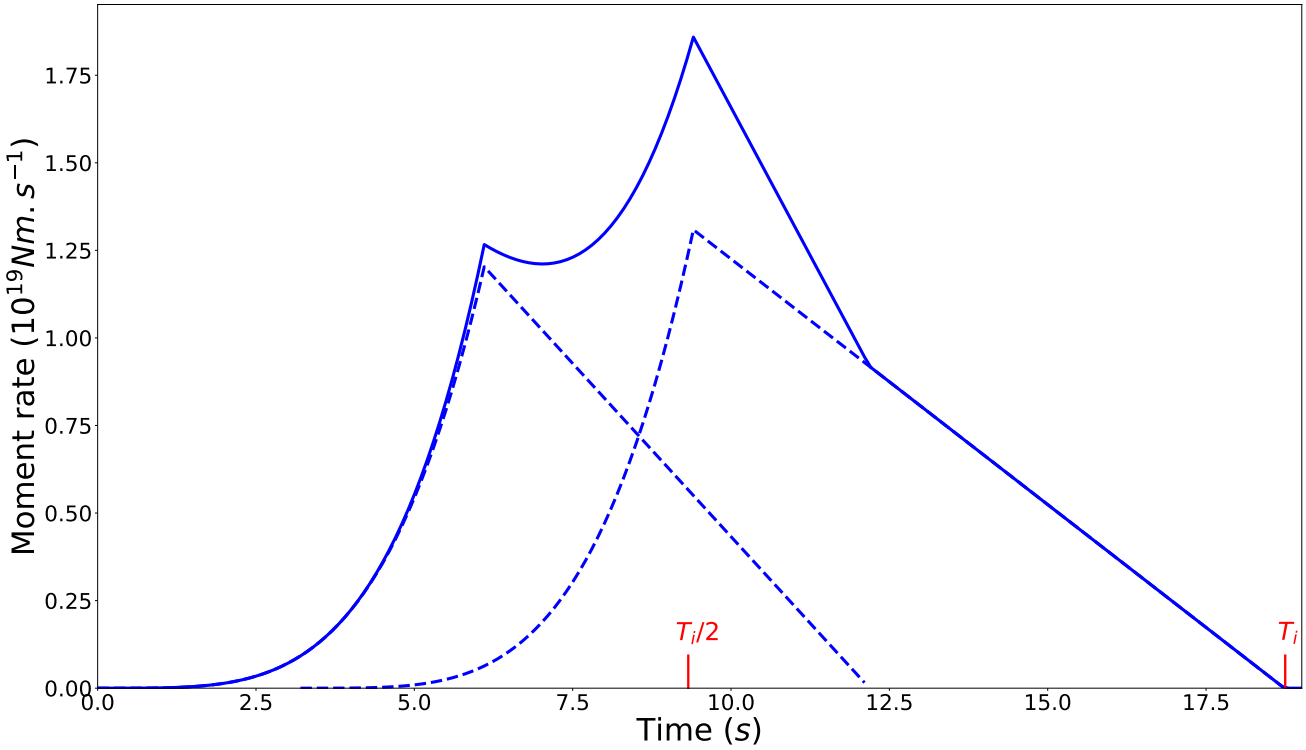

Figure S2. Example of the construction of a synthetic STF. Dashed blue lines represent each of the two sub-events, and the bold blue line is the sum of the two sub-events, i.e. the final synthetic STF. Red ticks show the half-duration and total duration of the STF.

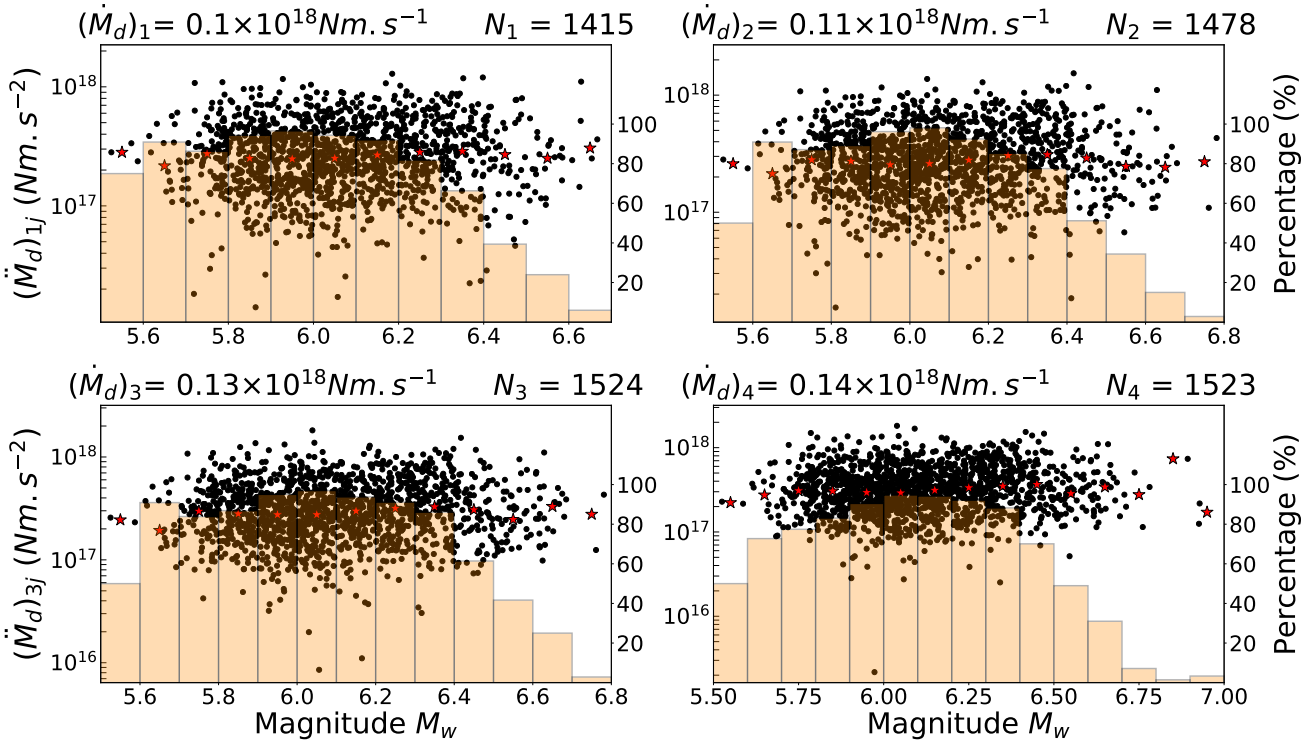

Figure S3. Moment acceleration as a function of magnitude for the four prescribed moment rates ($(\dot{M}_d)_1$ to $(\dot{M}_d)_4$). The filled histogram represents the ratio (in %) of sampled events per range of M_w.

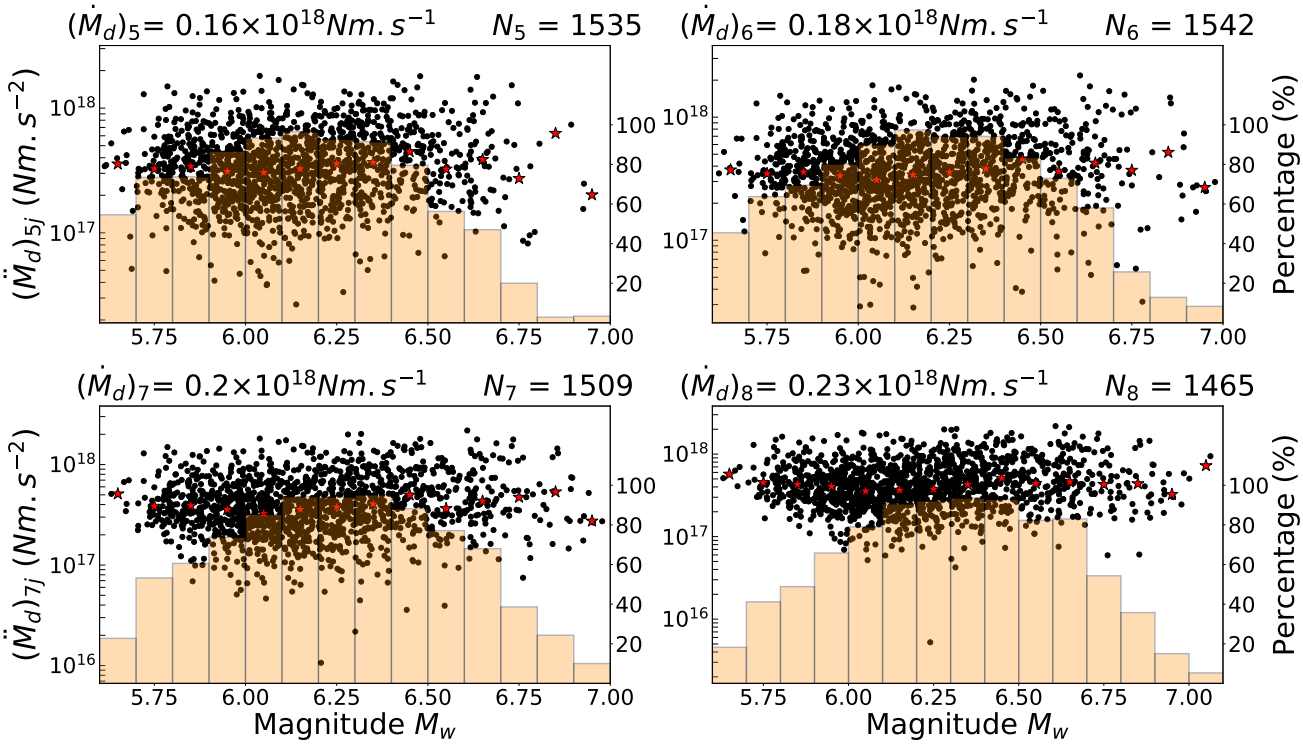

Figure S4. Moment acceleration as a function of magnitude for four prescribed moment rates ($(\dot{M}_d)_5$ to $(\dot{M}_d)_8$). The filled histogram represents the ratio (in %) of sampled events per range of M_w.

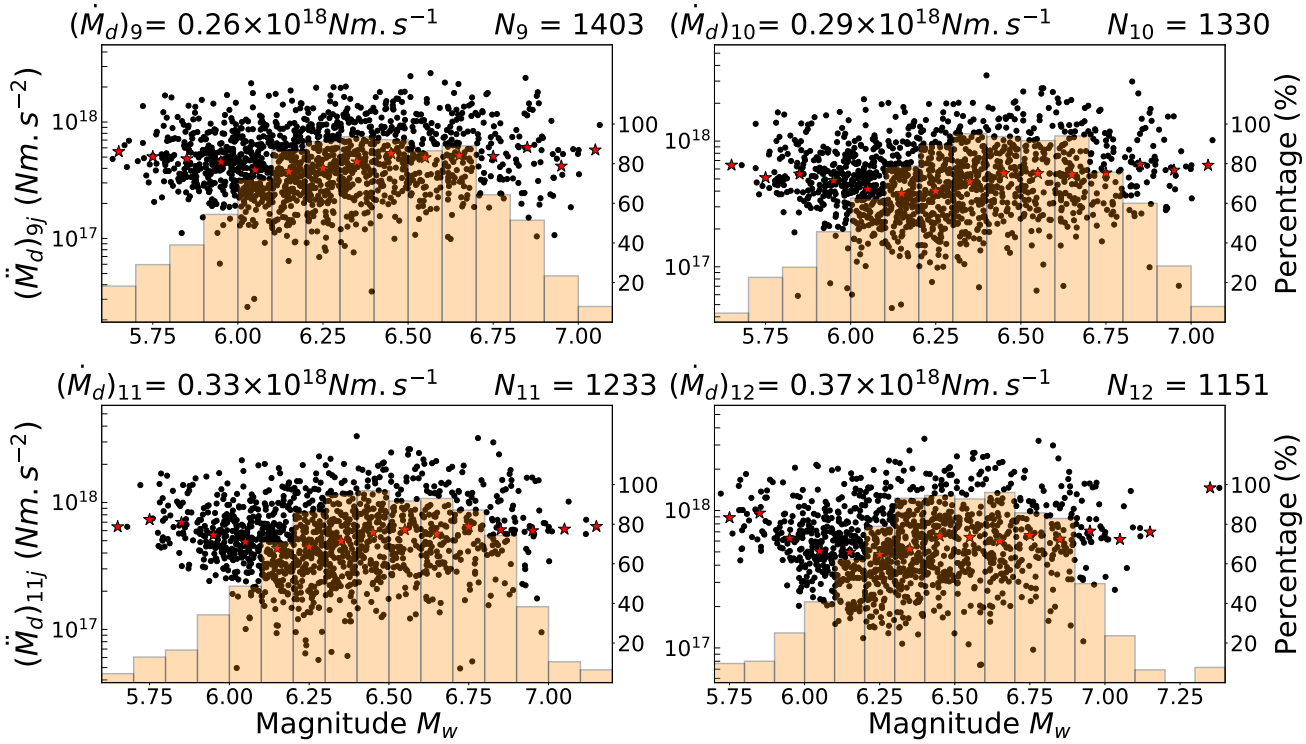

Figure S5. Moment acceleration as a function of magnitude for the four prescribed moment rates ($(\dot{M}_d)_9$ to $(\dot{M}_d)_{12}$). The filled histogram represents the ratio (in %) of sampled events per range of M_w.

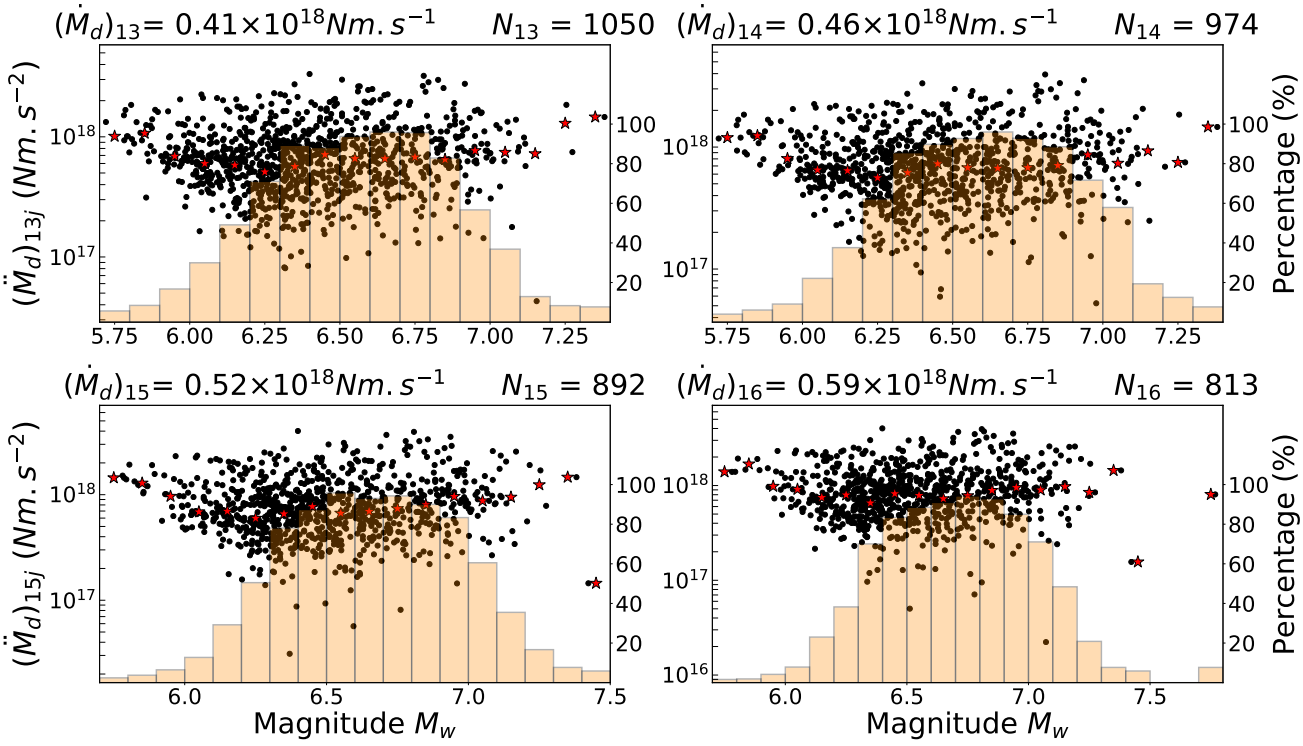

Figure S6. Moment acceleration as a function of magnitude for the four prescribed moment rates ($(\dot{M}_d)_{13}$ to $(\dot{M}_d)_{16}$). The filled histogram represents the ratio (in %) of sampled events per range of M_w.

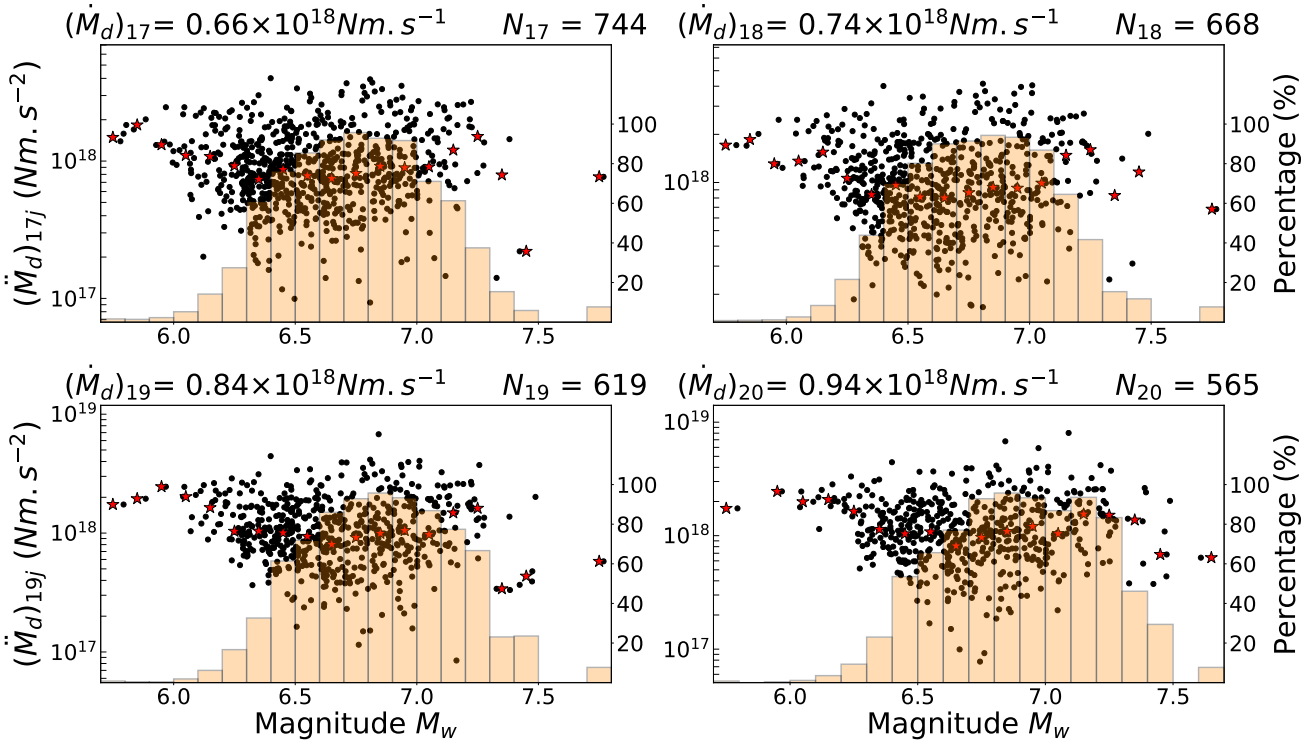

Figure S7. Moment acceleration as a function of magnitude for the four prescribed moment rates ($(\dot{M}_d)_{17}$ to $(\dot{M}_d)_{20}$). The filled histogram represents the ratio (in %) of sampled events per range of M_w.

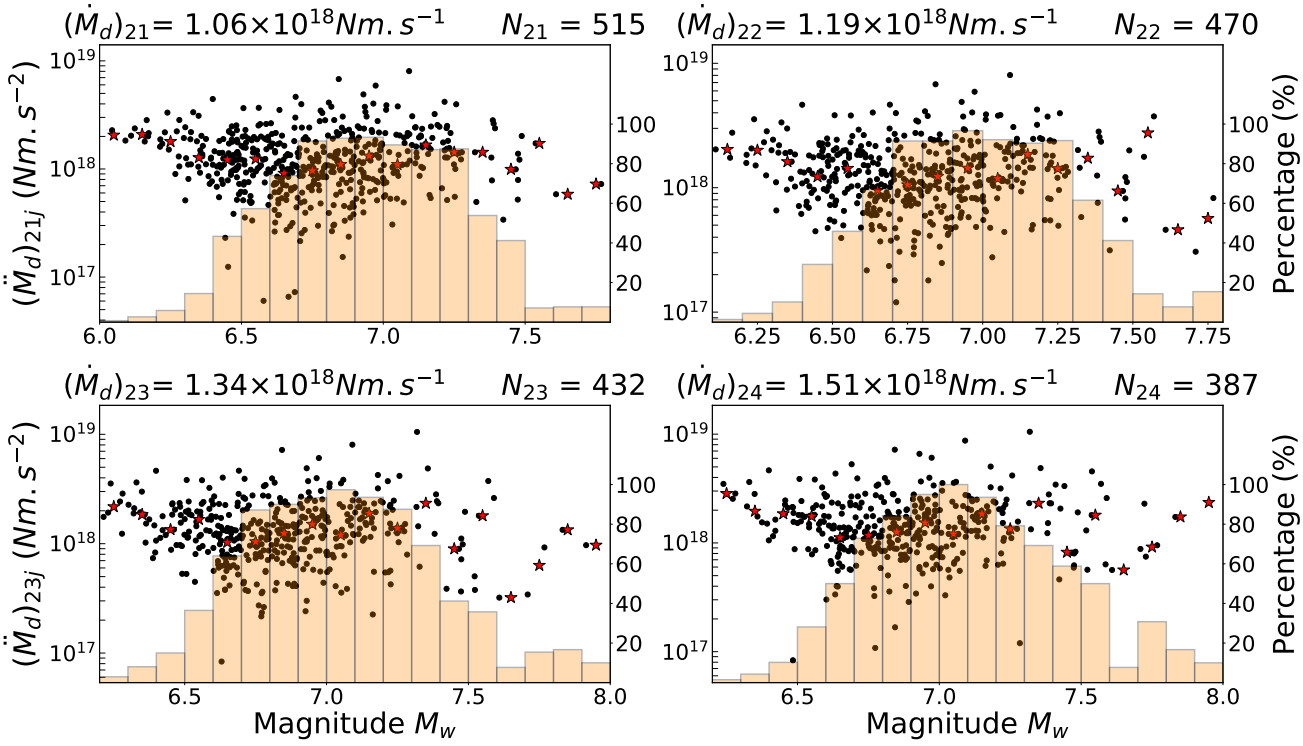

Figure S8. Moment acceleration as a function of magnitude for the four prescribed moment rates ($(\dot{M}_d)_{21}$ to $(\dot{M}_d)_{24}$). The filled histogram represents the ratio (in %) of sampled events per range of M_w.

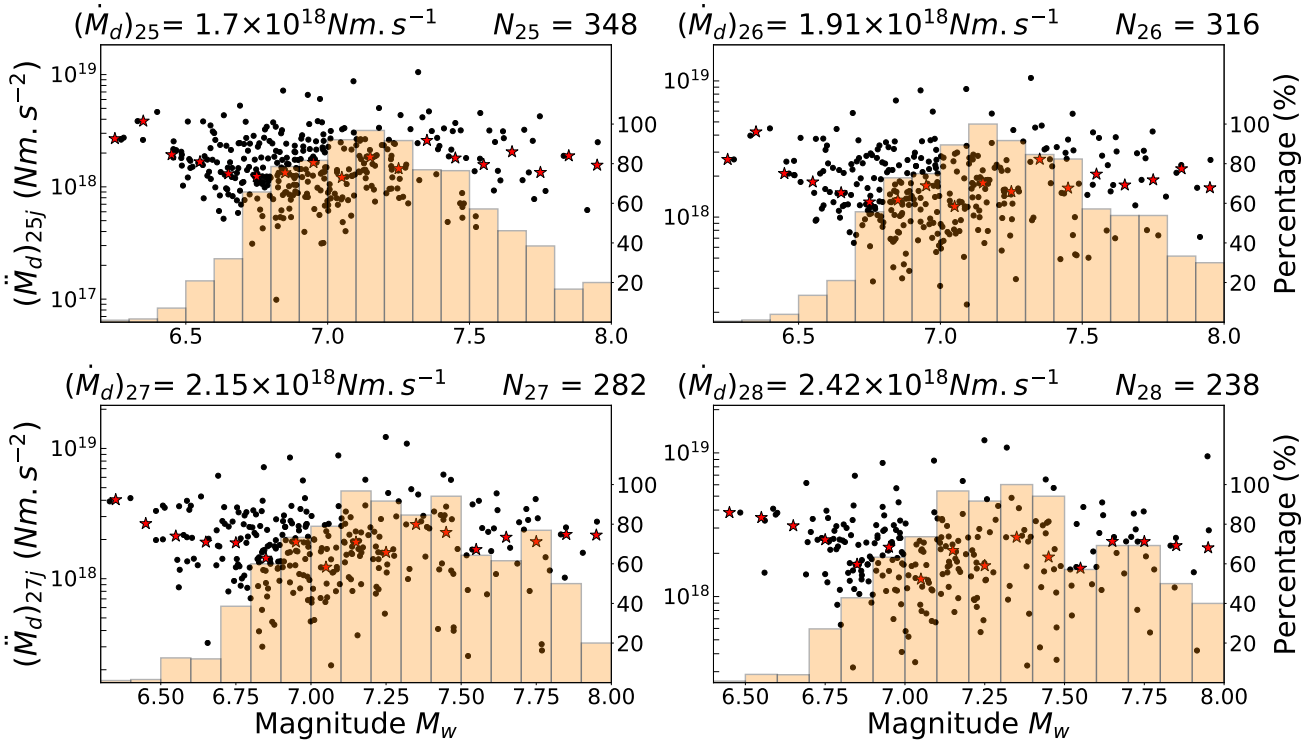

Figure S9. Moment acceleration as a function of magnitude for the four prescribed moment rates ($(\dot{M}_d)_{25}$ to $(\dot{M}_d)_{28}$). The filled histogram represents the ratio (in %) of sampled events per range of M_w.

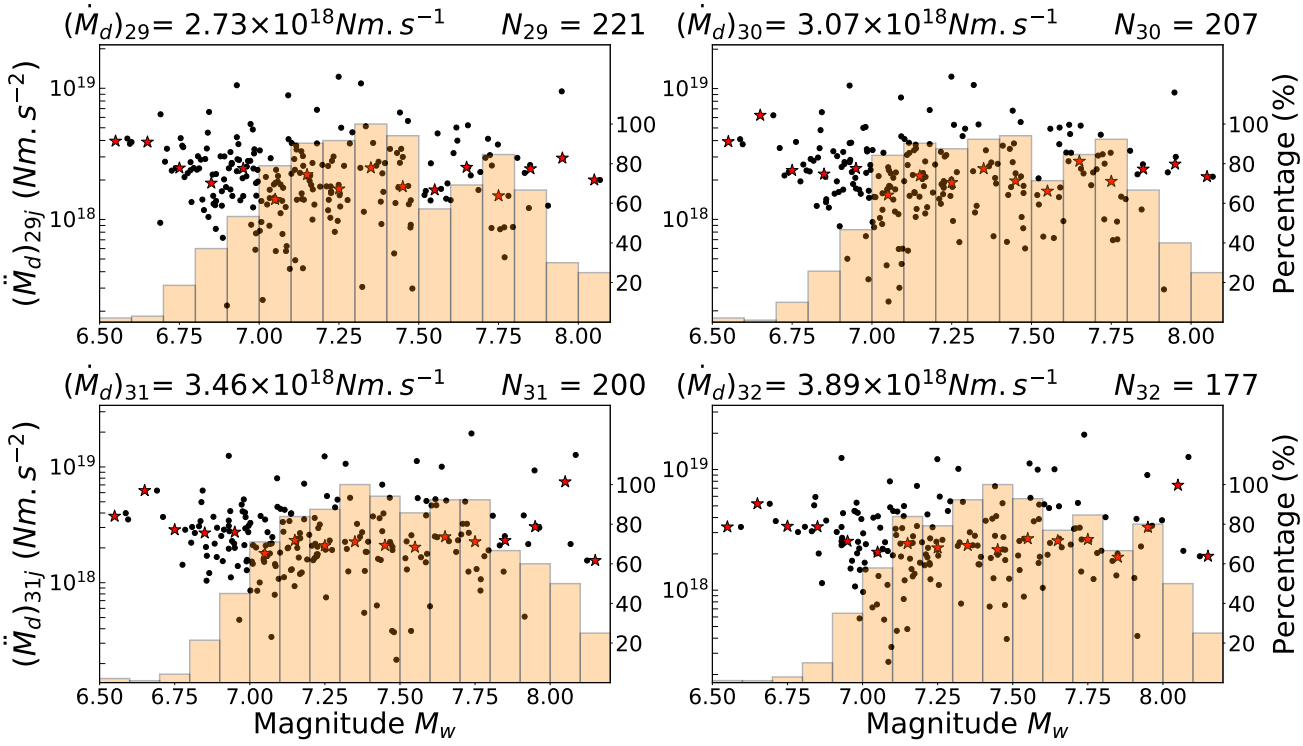

Figure S10. Moment acceleration as a function of magnitude for the four prescribed moment rates ($(\dot{M}_d)_{29}$ to $(\dot{M}_d)_{32}$). The filled histogram represents the ratio (in %) of sampled events per range of M_w.

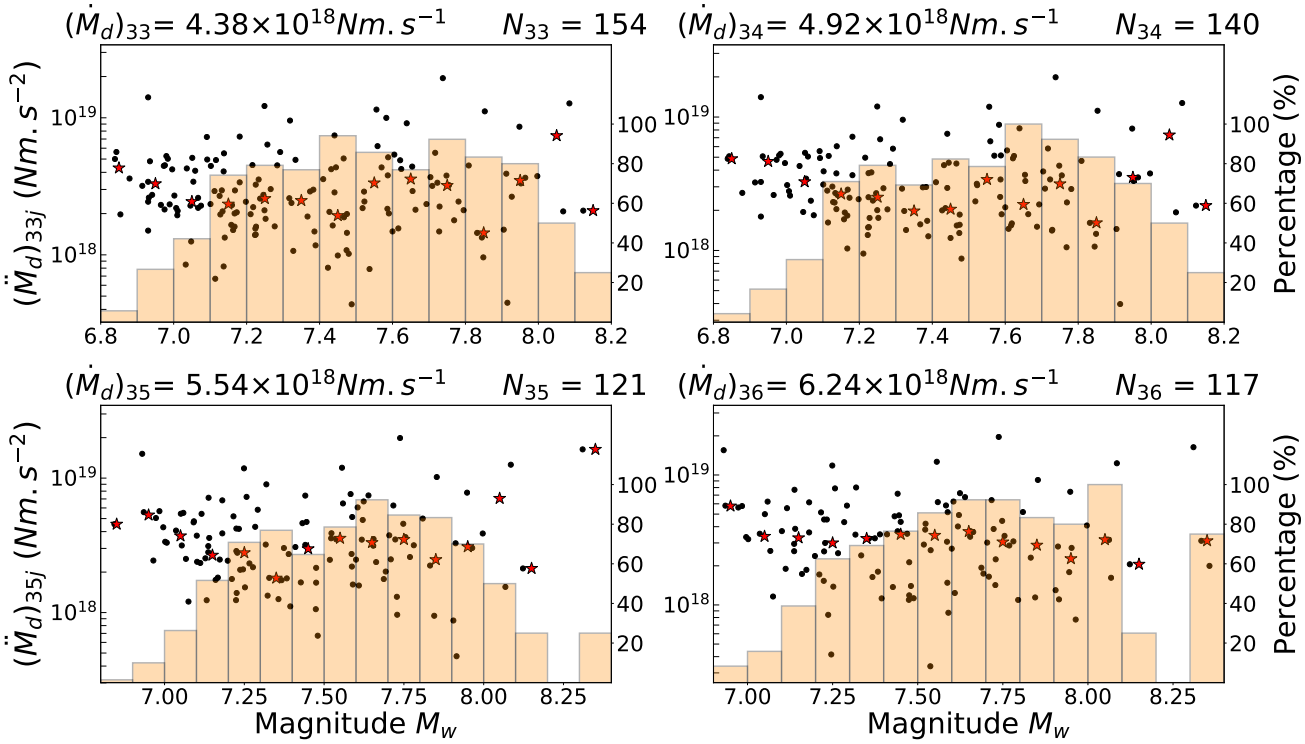

Figure S11. Moment acceleration as a function of magnitude for the four prescribed moment rates ($(\dot{M}_d)_{33}$ to $(\dot{M}_d)_{36}$). The filled histogram represents the ratio (in %) of sampled events per range of M_w.

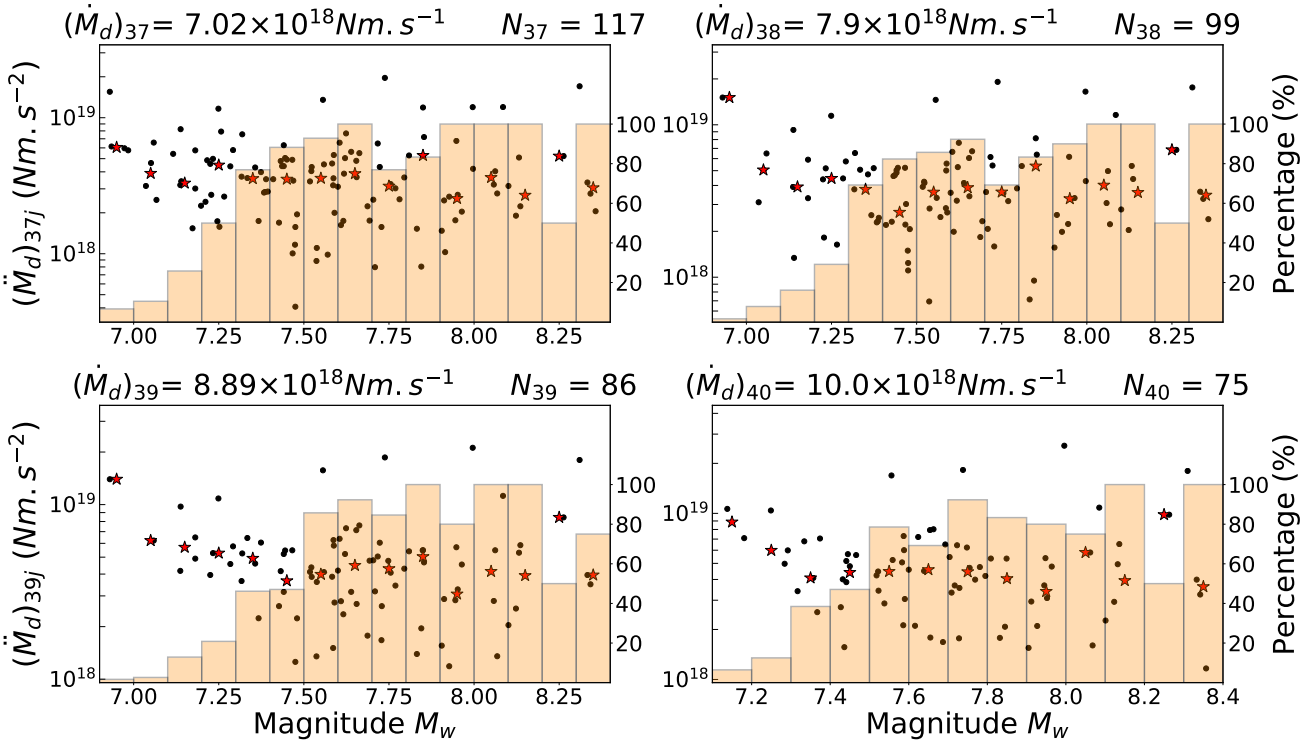

Figure S12. Moment acceleration as a function of magnitude for the four prescribed moment rates ($(\dot{M}_d)_{37}$ to $(\dot{M}_d)_{40}$). The filled histogram represents the ratio (in %) of sampled events per range of M_w.

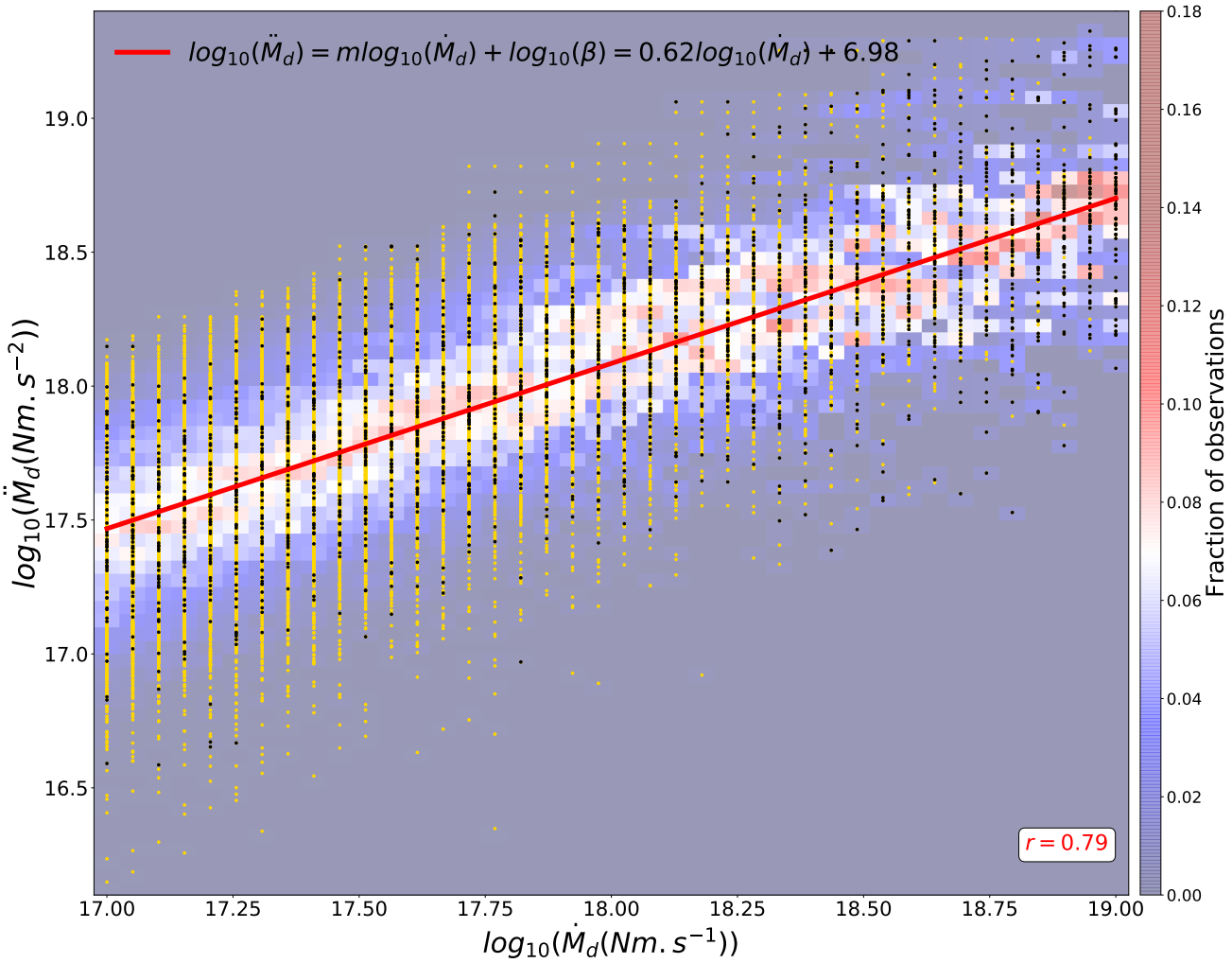

Figure S13. Same Figure as Figure 3 in the main text but with a development phase extracted between $0.05F_m$ and $0.5F_m$.